

# Noise analysis of spectrometers based on speckle pattern reconstruction

Brandon Redding,<sup>1</sup> Sebastien M. Popoff,<sup>1</sup> Yaron Bromberg,<sup>1</sup>  
Michael A. Choma,<sup>2,3</sup> and Hui Cao<sup>1,\*</sup>

<sup>1</sup>Department of Applied Physics, Yale University, New Haven, Connecticut 06520, USA

<sup>2</sup>Departments of Diagnostic Radiology and of Pediatrics, Yale School of Medicine, New Haven, Connecticut 06520, USA

<sup>3</sup>Department of Biomedical Engineering, Yale University, New Haven, Connecticut 06520, USA

\*Corresponding author: hui.cao@yale.edu

Received 16 October 2013; revised 13 December 2013; accepted 17 December 2013;  
posted 18 December 2013 (Doc. ID 199533); published 16 January 2014

Speckle patterns produced by a disordered medium or a multimode fiber can be used as a fingerprint to uniquely identify the input light frequency. Reconstruction of a probe spectrum from the speckle pattern has enabled the realization of compact, low-cost, and high-resolution spectrometers. Here we investigate the effects of experimental noise on the accuracy of the reconstructed spectra. We compare the accuracy of a speckle-based spectrometer to a traditional grating-based spectrometer as a function of the probe signal intensity and bandwidth. We find that the speckle-based spectrometers provide comparable performance to a grating-based spectrometer when measuring intense or narrowband probe signals, whereas the accuracy degrades in the measurement of weak or broadband signals. These results are important to identify the applications that would most benefit from this new class of spectrometer. © 2014 Optical Society of America

*OCIS codes:* (300.6190) Spectrometers; (120.6200) Spectrometers and spectroscopic instrumentation; (060.2370) Fiber optics sensors.

<http://dx.doi.org/10.1364/AO.53.000410>

## 1. Introduction

Traditional spectrometers rely on a grating or prism to provide one-to-one spectral to spatial mapping in which different wavelengths are mapped to different spatial positions. While these spectrometers have been used effectively in many applications, they have well-known limitations. For instance, the spectral resolution in a grating-based spectrometer scales with the optical path length, imposing a trade-off between device size and resolution. In recent years, more complex spectral-to-spatial mapping has been employed for spectrometer designs [1–6]. In these implementations, a dispersive medium maps different wavelengths to distinct spatial patterns rather

than localized positions. A calibration procedure is typically used to record the spatial pattern produced by each wavelength of interest. These patterns are used as a sort of “fingerprint” to uniquely identify an input wavelength and are stored in a transmission matrix. After calibration, recording the spatial pattern generated by an arbitrary probe signal is sufficient to reconstruct its spectrum in software. The advantage of this approach is that the grating or prism in a traditional spectrometer can be replaced by any kind of dispersive media, some of which have attractive features such as finer resolution in a given footprint, higher sensitivity, or lower cost.

This general approach has enabled spectrometers to be built using a disordered photonic crystal lattice [2], an array of Bragg fibers [1], or even a random structure [3,4]. Using a random medium is particularly attractive because the spectral resolution scales

as the square of the size of the random medium (in the multiple scattering regime where light transport is diffusive), enabling high resolution with a compact size. Recently, a random photonic nanostructure was used to develop a spectrometer on a silicon chip, where the trade-off between resolution and footprint is particularly restrictive [4]. The speckle pattern generated by interference of waveguided modes in a standard multimode optical fibers can also be used to build a spectrometer [5,6]. These all-fiber spectrometers combine high transmission with fine spectral resolution, which scales with the length of the fiber. Furthermore, commercial fibers are low cost, lightweight, and can be coiled into a small volume.

While these speckle-based spectrometers offer clear benefits in terms of size, weight, and cost, their sensitivity to experimental noise has not been fully investigated. Previous work on the photonic bandgap fiber bundle spectrometer considered several sources of noises, such as the discrete intensity resolution of a CCD array, the ambient light, and the variation of illumination condition of the bundle input facet by different light sources [1]. The biggest source of error in spectra reconstruction came from the difficulty in reproducing the same illumination conditions of the fiber bundle facet when constructing the transmission matrix and when characterizing the test spectra. This issue was eliminated in the spectrometer using a single multimode fiber, where light is always coupled through the same single-mode fiber into the multimode fiber [5,6]. It was also shown that the errors caused by the experimental noise can be multiplied by an ill-conditioned inversion procedure of the transmission matrix [1], and an effective measure of truncating small singular values below the noise level has been taken to improve the robustness of the reconstruction algorithm to experimental noise [1,4,5]. The detection noise seems important to the speckle-based spectrometer, because even a monochromatic signal would be spread over all detectors, but in a grating-based spectrometer it would be measured by a single detector. If the signal is weak or the detector noise is large (e.g., at the infrared frequency), dividing the signal over many detectors seems detrimental. Quantitatively, the performance depends on whether the shot noise of the signal or the dark noise of the detector is dominant.

A speckle-based spectrometer is similar to a Fourier transform (FT) spectrometer in the sense that light at different wavelengths contributes to the intensity measured on the same detector. This multiplexed detection has important implications regarding the regimes where FT spectrometers outperform grating-based spectrometers [7–9]. However, FT spectrometers have important distinctions compared to speckle-based spectrometers: FT spectrometers rely on a single detector element instead of an array, and require scanning to acquire a complete spectrum. Moreover, the reconstruction procedure is quite different, with speckle-based spectrometers relying on a matrix inversion procedure in

combination with a nonlinear optimization algorithm, rather than a FT.

In this work, we present a comprehensive analysis of the effects of shot noise and dark noise on the performance of the speckle-based spectrometers. Specifically, we consider the effects of the probe signal level, bandwidth, and the detector well-depth capacity on the spectral reconstruction error. For each parameter, the performance of the speckle-based spectrometer is compared to the expected performance of a grating-based spectrometer. Our analysis focuses on a multimode fiber spectrometer, but can be generalized to any speckle-based spectrometer.

This paper is organized as follows. Section 2 has a brief review of the operation principle of the speckle-based spectrometer. In Section 3, our approach to model shot noise and dark noise is introduced. In Section 4, we analyze the reconstruction error induced by the noise in a speckle-based spectrometer and compare to a grating-based spectrometer. Section 5 presents an experimental study of the spectral reconstruction error for a multimode fiber spectrometer. Finally, in Section 6, we discuss the implication of our results and conclude.

## 2. Transmission Matrix

The spectral–spatial mapping of a spectrometer is characterized by the transmission matrix,  $T$ , which relates the input spectrum,  $S$ , to the spatial intensity distribution,  $I$ , as  $I = T \cdot S$  [6]. For a grating-based spectrometer,  $T$  is an identity matrix, because every spectral channel is mapped to a single spatial channel. The transmission matrix for a speckle-based spectrometer is more complex, and it is generally measured experimentally during a calibration procedure, although in principle it could be calculated given precise knowledge of the dispersive element. After this calibration, the spectrometer operates by recording the intensity pattern generated by an unknown probe and then reconstructing its spectrum,  $S$ , given  $I$  and  $T$ . A direct approach to reconstruct the probe spectrum is simply to multiply the measured intensity pattern by the inverse of the transmission matrix:  $S = T^{-1} \cdot I$ . However, if the transmission matrix contains small singular values, the matrix inversion process is extremely sensitive to the experimental noise level [1,6]. The problem is easily understood if the matrix is first decomposed into singular values as  $T = U \cdot D \cdot V^T$ , where  $U$  and  $V$  are unitary matrices and  $D$  is a diagonal matrix with positive real elements  $D_{jj} = d_j$ , known as the singular values of  $T$ . The inverse of  $T$  is then given as  $T^{-1} = V \cdot D' \cdot U^T$  where  $D'$  is obtained by taking the reciprocal of each diagonal element in  $D$  and then taking the transpose. Thus the smallest singular values, which are most susceptible to noise, have the largest contributions to  $T^{-1}$ . To overcome this limitation, a “truncated” inversion procedure has been used in which the small singular values are discarded. The cutoff threshold below which singular values are discarded depends on

the experimental noise [1,6]. Alternately, the spectrum can be reconstructed without inverting the transmission matrix but instead relying on a nonlinear optimization algorithm. In this case, the algorithm searches for the spectrum,  $S$ , which minimizes  $\|T \cdot S - I\|^2$ , with the constraint that  $S$  is nonnegative. The nonlinear optimization often provides a more accurate spectrum; however, it is computationally more demanding. To reduce the computation time, the matrix inversion procedure can be used to provide an initial guess for the nonlinear optimization [6].

The dimension of a transmission matrix is defined by the number of spectral channels,  $M$ , and the number of spatial channels,  $N \cdot \delta\lambda$  is the spacing between neighboring spectral channels and the spectrometer bandwidth  $\Delta\lambda = \delta\lambda \cdot M$ . The spectral channels are not necessarily independent, namely, their speckle patterns may have some correlations. The degree of correlation is described by the spectral correlation function,  $C(\Delta\lambda, x) = \langle I(\lambda, x)I(\lambda + \Delta\lambda, x) \rangle / [\langle I(\lambda, x) \rangle \langle I(\lambda + \Delta\lambda, x) \rangle] - 1$ , where  $I(\lambda, x)$  is the intensity at position  $x$  for input wavelength  $\lambda$  and  $\langle \dots \rangle$  represents the average over  $\lambda$ . We then computed an average spectral correlation function over all positions,  $x$ , to obtain  $C(\Delta\lambda)$ . The spectral correlation width  $\delta\lambda_i$  is defined as  $C(\delta\lambda_i/2) = C(0)/2$ . If the channel spacing is equal to  $\delta\lambda_i$ , the spectral channels are independent. The number of spatial channels corresponds to the number of pixels of the camera used to record the intensity pattern. If the pixel size is much smaller than the average speckle size, the intensity recorded on nearby pixels is highly correlated [10], groups of neighboring pixels can be binned together to form a single detector channel. We therefore introduce an additional factor,  $\delta x$ , which describes the number of pixels that are binned together (in one dimension) to form one spatial channel. It also gives the distance of neighboring spatial channels. The spatial correlation width,  $\delta x_i$ , is obtained from the spatial correlation function  $C(\Delta x)$ , which is defined analogous to  $C(\Delta\lambda)$ . The spatial channels separated by  $\delta x_i$  are independent. The number of independent spatial channels  $N_i$  sets an upper limit for the number of independent spectral channels  $M_i$  that can be probed simultaneously.

As an example, we will consider a spectrometer based on a 1 meter long, standard step-index multimode fiber with a core diameter of 105  $\mu\text{m}$  and numerical aperture (NA) = 0.22. Experimentally, we coupled a tunable laser at  $\lambda = 1500$  nm through a single-mode, polarization-maintaining fiber to the multimode fiber. The speckle pattern at the output end of the multimode fiber consists of  $N_i = 500$  uncorrelated spatial modes with a spatial correlation width  $\delta x_i$  of 6 pixels. The spectral correlation width of the 1 meter long fiber was  $\delta\lambda_i = 0.4$  nm. We constructed a transmission matrix consisting of  $N = 2000$  spatial channels separated by 3 pixels and  $M = 500$  spectral channels separated by 0.2 nm, providing 100 nm of bandwidth from  $\lambda = 1450$  nm

to 1550 nm. By oversampling in the spatial domain, we added redundancy to the transmission matrix that improved the robustness of the reconstruction algorithm in the presence of noise. In the spectral domain, oversampling ensured that a probe signal centered in between the calibrated spectral channels would still produce a speckle pattern with strong correlation to the nearest calibrated speckle patterns. In the following sections, we will use this transmission matrix to compare the performance of a speckle-based spectrometer to a grating based spectrometer.

### 3. Modeling Noise

Compared to the one-to-one spectral-spatial mapping in a grating-based spectrometer, the complex spectral-spatial mapping of a speckle-based spectrometer may introduce additional noise from detection. As mentioned earlier, in a spectrometer based on fully developed speckle, the signal from any given wavelength is distributed over all the spatial channels, whereas in a spectrometer with a grating, the signal from one wavelength is concentrated on a single spatial channel. In Figs. 1(a) and 1(b), we present a sketch of the intensity measured on the

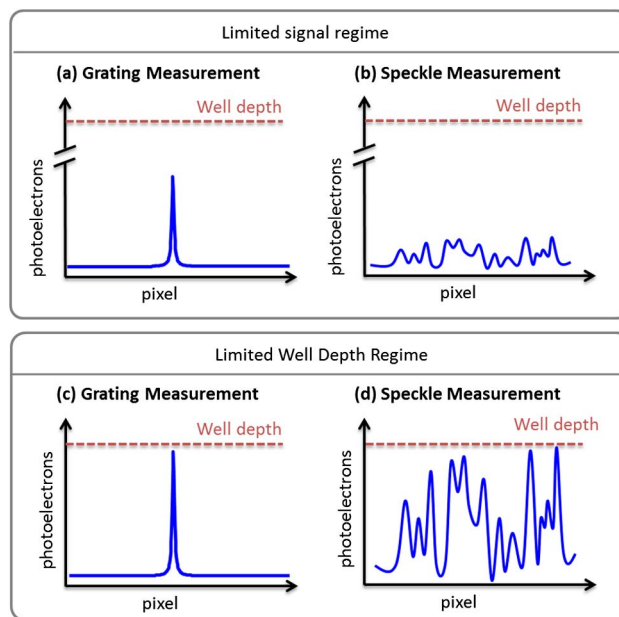


Fig. 1. Schematic of photoelectron distributions over the detector pixels for a narrowband signal in the limited signal regime (a), (b) and limited well-depth regime (c), (d). (a), (c) are for a grating-based spectrometer and (b), (d) for a speckle-based spectrometer. In the limited signal regime (a), (b), the total number of photoelectrons is fixed. The grating-based spectrometer maps all the photons at a given wavelength to a single detector, whereas the speckle-based spectrometer spreads them over all the detectors. In the limited well-depth regime (c), (d), the maximum number of photoelectrons in a single pixel reaches the well depth of the detector. By spreading light in a single spectral channel over all spatial channels, the speckle-based spectrometer allows many more photoelectrons to be created and detected without saturating any pixels.

detector array for the same narrowband probe signal in a grating-based spectrometer and a speckle-based spectrometer. Let us first compare the shot noise in these two cases. Assume the probe signal has  $N_p$  photons at a given wavelength. In the speckle-based spectrometer, the average number of photons in a single spatial channel is  $N_p/N$ . The shot noise in each spatial channel is  $\sqrt{N_p/N}$ , so the shot noise over all channels is  $\sqrt{N} \cdot \sqrt{N_p/N} = \sqrt{N_p}$ . In the grating-based spectrometer, all  $N_p$  photons hit a single detector, and the shot noise is  $\sqrt{N_p}$ . Hence, the shot noise is the same for a fixed number of input photons. The dark noise, however, is different, because in a grating-based spectrometer, the dark noise affecting the measurement of one spectral channel is limited to the dark noise of a single spatial detector, whereas in a speckle-based spectrometer, the dark noise is accumulated over all the detectors. This drawback is particularly pronounced in the case of weak optical signals. However, this difference in spectral-to-spatial mapping could also benefit the speckle-based spectrometer. If the signal is strong enough to fill the well depth of the detector, then the speckle-based spectrometer allows many more total photoelectrons to be created by spreading the signal over all the detectors, as indicated in Figs. 1(c) and 1(d). This is particularly relevant in applications where the camera frame rate limits the data acquisition rate. For example, in applications requiring high-speed spectral measurements (e.g., spectral domain optical coherence tomography), the camera is often operating close to the maximum frame rate, and thus a speckle-based spectrometer could collect more photoelectrons per frame. To illustrate this difference, we will consider two operating regimes, which we call the limited signal regime and the limited well-depth regime. In the limited signal regime, the total number of photoelectrons integrated over all wavelengths is fixed. In the limited well-depth regime, the maximum number of photoelectrons in individual detectors just reaches the well depth without saturating any detector. In the next section, we will compare the reconstruction error in these two regimes as a function of the signal intensity and bandwidth.

In a grating-based spectrometer, the intensity measured on a given detector (i.e., a pixel or group of pixels) is directly proportional to the amplitude of the probe signal in a given spectral band. As a result, the accuracy of the spectral measurement is directly related to the shot noise of the signal and the dark noise of the detector. However, in a speckle-based spectrometer, it is less clear how noise from the detection propagates through the reconstruction process to manifest as noise in the reconstructed spectrum. This problem is particularly challenging when the reconstruction process relies on a nonlinear optimization routine. In order to model the reconstruction error in a speckle-based spectrometer we developed the following procedure:

(1) **Construct a transmission matrix.** In the following analysis, we consider a transmission matrix  $T$  recorded experimentally using a 1 m long multimode fiber with a 105  $\mu\text{m}$  diameter core and  $\text{NA} = 0.22$ . As discussed in section 2,  $T$  contains  $N = 2000$  spatial channels and  $M = 500$  spectral channels. The multimode fiber spectrometer provided 100 nm of bandwidth, from  $\lambda = 1450$  to 1550 nm in steps of 0.2 nm. The matrix was measured by setting the wavelength of a tunable laser to each spectral channel and recording the speckle pattern produced at the end of the multimode fiber [5,6]. The noise in the measurement of the transmission matrix is ignored, since  $T$  can be measured many times and averaged to reduce noise to an arbitrary level.

(2) **Choose a probe spectrum.** Initially, we study the reconstruction error when measuring a single narrow line with the Lorentzian shape and bandwidth of 1 nm. Later, we investigate the reconstruction error for probe signals with varying bandwidth.

(3) **Compute the speckle pattern without noise.** We then calculate the “ideal” speckle pattern that we would expect to measure in the absence of any noise. This speckle pattern is computed as  $I = T \cdot S$ , where  $S$  is the probe spectrum selected above.

(4) **Introduce noise to the detected speckle pattern.** We then introduce noise to the “ideal” speckle pattern. We include two noise terms in our analysis: shot noise and dark noise. In this step, we add random noise to every spatial channel as  $I'_j = I_j + \sigma_j + \delta_j$ , where  $I_j$  is the ideal number of photoelectrons recorded on spatial channel  $j$ , and  $I'_j$  is the number of photoelectrons measured in the presence of shot noise,  $\sigma_j$ , and dark noise,  $\delta_j$ .  $\langle \sigma_j \rangle = 0$ ,  $\langle \delta_j \rangle = 0$ ,  $\langle I'_j \rangle = \langle I_j \rangle$ . Note that the shot noise and dark noise in each spatial channel were uncorrelated with each other and with the noise in all other channels. The shot noise on a given channel was taken as a random number with a Gaussian distribution with the full width at half-maximum (FWHM) proportional to the square root of the mean number of photoelectrons  $\langle I_j \rangle$ , such that the standard deviation of  $\sigma_j$  was equal to  $\langle I_j \rangle^{1/2}$ . The dark noise was taken as a random number with a Gaussian distribution whose FWHM was set to  $10^3$  photoelectrons, corresponding to the dark noise measured experimentally on our camera (Xenics Xeva-1.7-320), which had a full well depth of  $\sim 10^6$  photoelectrons. By varying the intensity of the probe signal,  $S$ , we were able to test the ability of the speckle-based spectrometer to reconstruct the input spectra in the presence of varying levels of noise.

(5) **Reconstruct the probe spectrum.** We then attempt to reconstruct the probe spectrum using the intensity pattern perturbed by noise,  $I'$ , and the original transmission matrix,  $T$ . We first use a matrix inversion procedure to estimate the probe spectrum as  $S' = T^{-1} \cdot I'$ , where  $S'$  is the reconstructed spectrum in the presence of noise. We then seed this  $S'$

to a nonlinear optimization algorithm that searches for the spectrum that minimizes  $\|I' - T \cdot S'\|^2$  [6].

(6) **Evaluate the reconstruction error.** In order to evaluate the accuracy of the spectral reconstruction in the presence of noise, we used the standard deviation of the measured spectrum from the ideal spectrum as the metric. The normalized standard deviation,  $\mu$ , is defined as  $\mu = \sqrt{M^{-1} \sum_{\lambda} [S(\lambda) - S'(\lambda)]^2 / (M^{-1} \sum_{\lambda} [S(\lambda)]^2)}$  where  $S$  is the original probe spectrum,  $S'$  is the reconstructed spectrum in the presence of noise.

For each probe spectrum, we repeat the above procedure 10 times to account for variations in the randomly generated shot noise and dark noise and compute the average reconstruction error. We also compute the error expected using a grating-based spectrometer with identical spectral resolution and bandwidth. For a grating-based spectrometer, the deviation of the measured spectrum from the ideal spectrum is directly proportional to the detection noise at each wavelength.

#### 4. Spectra Reconstruction Error

We first considered the reconstruction error when measuring a narrow probe spectrum in the limited signal regime. The probe signal is centered at  $\lambda = 1500$  nm and has a Lorentzian shape of 1 nm FWHM. We varied the total number of photoelectrons produced by the probe signal from  $10^4$  to  $10^8$ , calculated the reconstruction error for the speckle-based spectrometer, and compared to a grating-based spectrometer. Figures 2(a) and 2(b) show the reconstructed spectra at three photoelectron levels. The spectra were normalized by the maximum intensity and offset vertically for clarity. When the signal is sufficiently strong, both the speckle-based and the grating-based spectrometers provide an accurate measure of the spectrum. This is because the shot noise dominates over the dark noise, and the shot noise is the same for the two types of spectrometers at a fixed signal level. Since the noise is much lower than the signal, the spectral reconstruction is nearly unaffected by the presence

of noise. As the signal becomes weaker, the error in the spectrum measured with the speckle-based spectrometer degrades more rapidly. This is because the dark noise becomes more significant, and it has stronger contribution to the speckle-based spectrometer. In Fig. 2(c), we plot the reconstruction error as a function of the signal level. In the case of the speckle-based spectrometer, once the average signal on the detector channels approaches the dark noise, the reconstructed spectrum is no longer accurate. In the case of the grating-based spectrometer, the signal is concentrated on only a few detectors and remains above the dark noise on these detectors at substantially lower levels of total signal.

We then considered the same narrowband signal in the limited well-depth regime. In this case, we varied the well depth of the detectors and increased the total signal level as much as possible without saturating any of the detectors. As a result, the speckle-based spectrometer collected significantly more photoelectrons than the grating-based spectrometer by spreading the signal across all the detectors, as shown in Fig. 1(d). Figures 3(a) and 3(b) present reconstructed spectra at three well depths for the two spectrometers. The reconstruction error,  $\mu$ , is plotted as a function of well depth in Fig. 3(c). In the limited well-depth regime, the speckle-based spectrometer has similar accuracy as the grating-based spectrometer, and, at some well depths, the speckle-based spectrometer actually provides a more accurate measurement. The ability of the speckle-based spectrometer to spread the signal over many spatial channels and thereby produce more photoelectrons without saturation makes it well suited for applications requiring the accurate measurement of narrowband continuous-wave signals.

In a speckle-based spectrometer, the accuracy of spectral measurement depends on probe bandwidth. Since different spectral channels produce uncorrelated speckle patterns that add in intensity, the speckle contrast decreases with increasing bandwidth. When the speckle contrast approaches the noise level, the spectra cannot be reconstructed accurately [6]. In a grating-based spectrometer, each

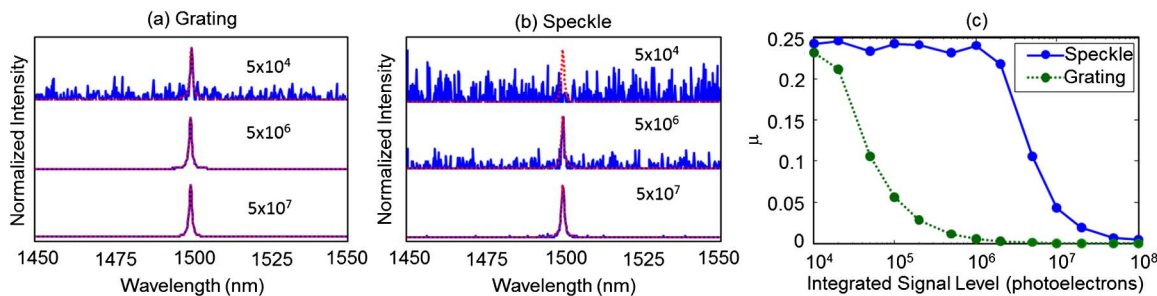


Fig. 2. Reconstructed spectra for a narrowband probe in the *limited signal regime* using a grating-based spectrometer (a) or a speckle-based spectrometer (b) at three different signal levels (the total number of photoelectrons is marked next to each curve). The ideal probe spectra are plotted by the red-dotted lines and the measured spectra in the presence of noise by the blue solid lines. (c) Spectral reconstruction error,  $\mu$ , as a function of signal level integrated over all wavelengths for the two types of spectrometers. The grating-based spectrometer is able to accurately measure the spectrum for signals about two orders of magnitude weaker than the speckle-based spectrometer in the limited signal regime.

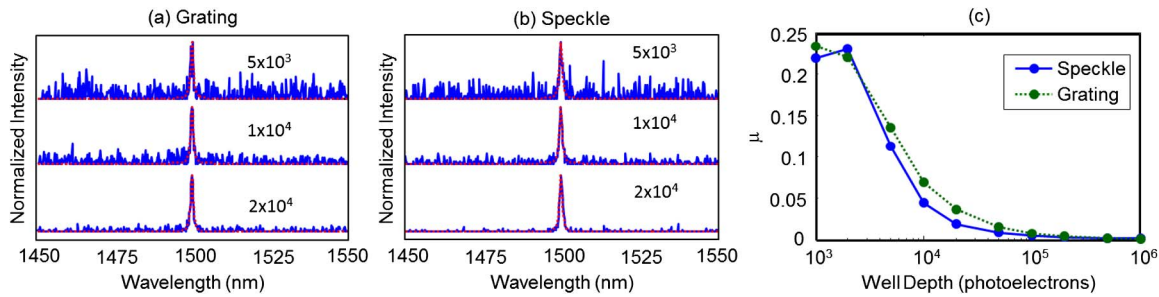


Fig. 3. Reconstructed spectra for a narrowband probe in the *limited well-depth regime* using a grating-based spectrometer (a) or speckle-based spectrometer (b) at three different detector well depths (indicated next to the curve). The ideal probe spectra are plotted by the red-dotted lines and the measured spectra in the presence of noise by the blue solid lines. (c) Reconstruction error,  $\mu$ , as a function of the detector well depth for the two types of spectrometers. The speckle-based spectrometer provides slightly more accurate measurements than the grating-based spectrometer for narrowband probes in the limited well-depth regime.

spectral channel is measured by a separate detector; thus the measurement accuracy is barely affected by the probe bandwidth. To analyze this effect, we studied the reconstruction error for probe signals with varying bandwidth, defined by the FWHM of a Lorentzian probe.

We first considered the limited signal regime with the total number of photoelectrons fixed at  $10^7$ . Figures 4(a) and 4(b) show the reconstructed spectra using the grating-based and speckle-based spectrometers for probe signals of increasing bandwidth. While the grating spectrometer accurately measures each probe spectra, the accuracy of the spectra reconstructed by the speckle-based spectrometer degrades at larger bandwidth. In Fig. 4(c), we plot the reconstruction error  $\mu$  for probe signals with bandwidth ranging from 1 to 40 nm. While the error for the grating-based spectrometer was relatively unaffected by the probe bandwidth, the error of the speckle-based spectrometer increases with bandwidth.

We then performed the same study of reconstruction error as a function of probe bandwidth in the limited well-depth regime. The detector well depth was fixed at  $10^6$  photoelectrons. Figures 5(a) and 5(b) show the reconstructed spectra of the grating-based and speckle-based spectrometers for three probe bandwidths. The reconstruction error,  $\mu$ , is plotted as a function of probe bandwidth in

Fig. 5(c). Although the speckle-based spectrometer outperformed the grating-based spectrometer in the limited well-depth regime for a narrowband probe, as shown in Fig. 3(c), the grating-based spectrometer is clearly more accurate when measuring broadband probes. As mentioned earlier, the speckle-based spectrometer spreads a narrowband probe signal over all spatial channels, producing significantly more photoelectrons in the limited well-depth regime. However, as the probe bandwidth increased, more and more spectral channels produce photoelectrons at each detector; with the fixed well depth, the contribution from each spectral channel is reduced. Thus the accuracy of reconstructing each spectral channel is lower at larger bandwidth. Although we considered continuous Lorentzian probes in Figs. 4 and 5, we expect the same trends to hold for any spectral shape with a similar number of spectral channels. That is, as the number of spectral channels in the probe increases, the reconstruction error for the speckle-based spectrometer will also increase.

## 5. Experimental Reconstruction Error

To validate the above noise analysis, we conducted an experimental study on the reconstruction error of a multimode-fiber spectrometer whose transmission matrix was used in the noise analysis in the previous section. After calibrating the transmission

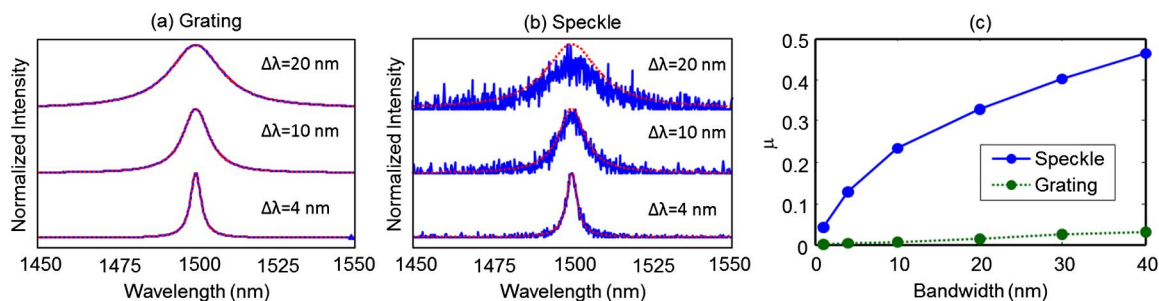


Fig. 4. Reconstructed spectra for probes with varying bandwidth (indicated by the FWHM,  $\Delta\lambda$ ) in the *limited signal regime* using a grating-based spectrometer (a) or a speckle-based spectrometer (b). The ideal probe spectra are plotted by the red-dotted lines and the measured spectra in the presence of noise by the blue solid lines. (c) Comparison of the reconstruction error,  $\mu$ , as a function of the signal bandwidth for the two types of spectrometers. The total number of photoelectrons over all spectral channels is set to  $10^7$ . The grating-based spectrometer displays better accuracy in the limited signal regime, especially for broadband signals.

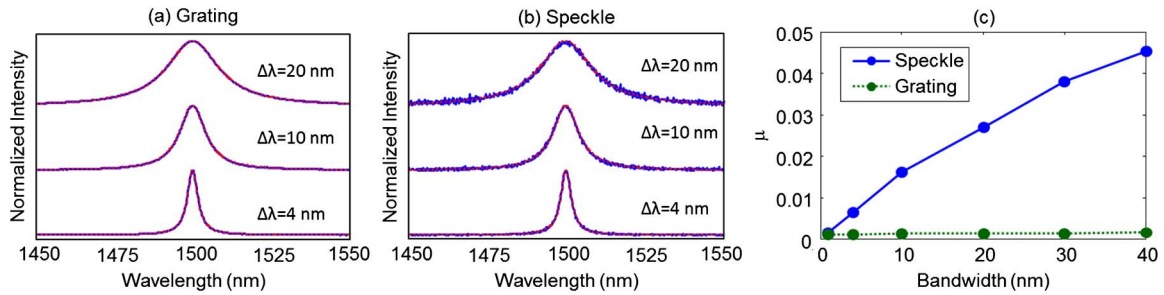


Fig. 5. Reconstructed spectra for probes with varying bandwidth (indicated by the FWHM,  $\Delta\lambda$ ) in the *limited well-depth regime* using a grating-based spectrometer (a) or transmission matrix based spectrometer (b). The ideal probe spectra are plotted by the red-dotted line and the measured spectra in the presence of noise by the blue solid line. (c) Comparison of the reconstruction error,  $\mu$ , as a function of signal bandwidth for the two types of spectrometers. The detector well depth is set to  $10^6$  photoelectrons. For the narrowband spectra, the speckle-based spectrometer has similar accuracy to the grating-based spectrometer; however, the accuracy of the speckle-based spectrometer degrades with bandwidth while the grating-based spectrometer is relatively unaffected in the limited well-depth regime.

matrix, we recorded a series of speckle patterns at a fixed probe wavelength of  $\lambda = 1500$  nm as we varied the signal intensity. Since these measurements were recorded well below the camera well depth, this experiment corresponds to the limited signal regime discussed above. Figures 6(a)–6(d) show the speckle patterns recorded at different laser powers (the total number of photoelectrons in each speckle pattern is indicated). As the signal level decreases, the number of photoelectrons generated in each pixel approaches the dark noise level of the camera, and the speckle pattern becomes less distinguishable. In Fig. 6(e), we present the spectra reconstructed from the measured speckle patterns in Figs. 6(a), 6(b), and 6(d). Using the speckle pattern in Fig. 6(a), which was recorded at  $\sim 1/10$ th of the camera well depth, the spectra is reconstructed nearly perfectly. As the signal level was further reduced, the fiber spectrometer continued to accurately

recover the probe spectrum, despite a gradual increase in the background noise. Remarkably, the peak wavelength of the probe signal can still be identified from the speckle pattern in Fig. 6(d), in which only a few speckles remain above the dark noise level. In Fig. 6(f), we plot the spectral reconstruction error  $\mu$  as a function of the total signal level. We also simulated  $\mu$  using the procedure outlined above for the same narrowband probe. As seen in Fig. 6(f), the simulated error is in good agreement to the experimentally measured error, validating our approach to modeling the noise in a speckle-based spectrometer.

## 6. Discussion and Conclusion

We note that our model neglected any noise sources related to the instability of the dispersive medium, since it inherently depends on the implementation. In the case of a multimode-fiber spectrometer, the

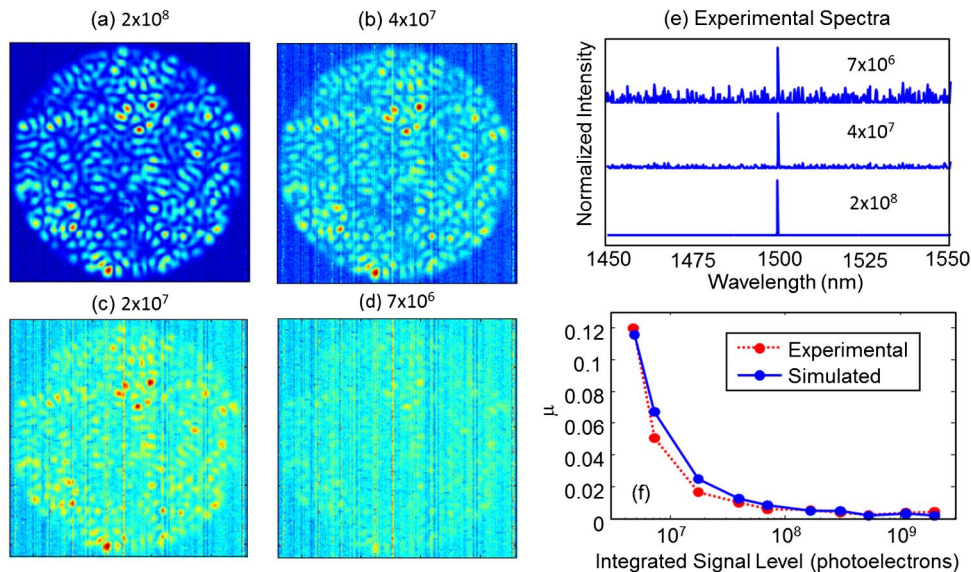


Fig. 6. (a)–(d) Experimental speckle patterns produced by a multimode fiber at  $\lambda = 1500$  nm at four levels of signal power in the limited signal regime. The total number of photoelectrons in each pattern is written on the top. (e) Spectra reconstructed from speckle patterns in (a), (b), (d). Even with only  $7 \times 10^6$  photoelectrons, corresponding to the barely visible speckle pattern in (d), the peak wavelength of the probe signal is accurately identified. (f) Experimentally measured and numerically simulated spectral reconstruction error  $\mu$  as a function of the total signal level (integrated over all detectors).

fiber must be mechanically fixed after calibration. In addition, a significant change in temperature also compromises the calibration [6]. The sensitivity to these environmental fluctuations typically scales with the resolution of the spectrometer: the higher the resolution, the more sensitive to environmental changes. Despite neglecting this potential source of noise, the error in the reconstructed spectrum when accounting for only shot noise and dark noise successfully predicted the measurement accuracy for a 1 m-long fiber spectrometer. In this experiment, the multimode fiber was placed on an optics table and undisturbed during testing, but no mechanical or thermal stabilization was required to provide accurate measurements after calibration.

The noise analysis presented above helps to identify applications that are most suitable to a speckle-based spectrometer. As discussed in the introduction, the versatility of the complex spectral-spatial mapping approach allows spectrometers to be very compact, high resolution, and low cost. However, these advantages are associated with clear trade-offs, as shown in Section 3. For instance, a speckle-based spectrometer is probably not the ideal choice for applications that measure weak broadband signals. However, in applications requiring accurate identification of narrowband or relatively strong signals, speckle-based spectrometers perform well. For example, the ability to accurately identify a narrow line could be useful in wavemeter applications or as a monitor in telecommunications, to determine which spectral channels are in use.

In summary, we investigated the effects of shot noise and dark noise on the spectral reconstruction error of the speckle-based spectrometers. We compared the accuracy of a speckle-based spectrometer to a grating based spectrometer as a function of signal level and bandwidth in the regimes of operation limited by the signal level or the detector well depth. Finally, we validated our model by comparison with the error in spectra reconstructed from experimentally measured speckle patterns at

varying signal levels. Although a multimode fiber spectrometer was used as an example in our analysis, we believe the conclusions are general to a wide range of spectrometers based on fully developed speckle. Our analysis shows that in applications requiring the measurement of strong or narrowband probe signals, speckle-based spectrometers provide comparable accuracy to grating-based spectrometers. In addition, speckle-based spectrometers can be substantially more compact, lighter weight, and lower cost than traditional grating based spectrometers of similar resolution.

We thank Profs. Paul Fleury and A. Douglas Stone for useful discussions. This work was supported in part by the National Science Foundation under the Grant No. ECCS-1128542.

## References

1. Q. Hang, B. Ung, I. Syed, N. Guo, and M. Skorobogatiy, "Photonic bandgap fiber bundle spectrometer," *Appl. Opt.* **49**, 4791–4800 (2010).
2. Z. Xu, Z. Wang, M. Sullivan, D. Brady, S. Foulger, and A. Adibi, "Multimodal multiplex spectroscopy using photonic crystals," *Opt. Express* **11**, 2126–2133 (2003).
3. T. W. Kohlgraf-Owens and A. Dogariu, "Transmission matrices of random media: means for spectral polarimetric measurements," *Opt. Lett.* **35**, 2236–2238 (2010).
4. B. Redding, S. F. Liew, R. Sarma, and H. Cao, "Compact spectrometer based on a disordered photonic chip," *Nat. Photonics* **7**, 1–6 (2013).
5. B. Redding and H. Cao, "Using a multimode fiber as a high-resolution, low-loss spectrometer," *Opt. Lett.* **37**, 3384–3386 (2012).
6. B. Redding, S. M. Popoff, and H. Cao, "All-fiber spectrometer based on speckle pattern reconstruction," *Opt. Express* **21**, 6584–6600 (2013).
7. P. B. Fellgett, "On the ultimate sensitivity and practical performance of radiation detectors.," *J. Opt. Soc. Am.* **39**, 970–976 (1949).
8. P. B. Fellgett, "The multiplex advantage," Ph.D. Thesis (University of Cambridge, 1951).
9. T. Hirschfeld, "Fellgett's advantage in uv-VIS multiplex spectroscopy," *Appl. Spectrosc.* **30**, 68–69 (1976).
10. J. W. Goodman, *Speckle Phenomena in Optics* (Roberts & Company, 2007).